General Disclaimer

One or more of the Following Statements may affect this Document

- This document has been reproduced from the best copy furnished by the organizational source. It is being released in the interest of making available as much information as possible.

- This document may contain data, which exceeds the sheet parameters. It was furnished in this condition by the organizational source and is the best copy available.

- This document may contain tone-on-tone or color graphs, charts and/or pictures, which have been reproduced in black and white.

- This document is paginated as submitted by the original source.

- Portions of this document are not fully legible due to the historical nature of some of the material. However, it is the best reproduction available from the original submission.

NINTH QUARTERLY REPORT

ON

"SPECTRORADIOMETRIC CALIBRATION OF THE THEMATIC MAPPER AND MULTISPECTRAL SCANNER SYSTEM"

Contract Number NAS5-27382
For the Period: 1 November 1984 through 28 February 1985

James M. Palmer, Co-Investigator
Philip N. Slater, Principal Investigator

Optical Sciences Center
University of Arizona
Tucson, Arizona 85721

INTRODUCTION

This is the ninth quarterly report on contract NAS5-27382 entitled "Spectroradiometric Calibration of the Thematic Mapper and Multispectral Scanner System".

The body of this report is a chapter from Carol J. Kastner's dissertation on atmospheric models. During her recent seminar at Goddard Space Flight Center, this material proved to be of interest to several in attendance.

Work on the reduction of data for the October 28, 1984 TM overpass of White Sands has produced some unexpected results. We are presently involved in relating the TM calibration data to three other quantities: the data from the calibrated radiometer in the helicopter, diffuse to direct irradiance collected at the ground and path radiance estimates determined from the imagery in water areas and cloud shadow areas. The results of this analysis will be presented in the next report.

CHAPTER 4

MODEL ATMOSPHERES

To calibrate an in-orbit sensor using ground based measurements, the effects of the atmosphere on propagating radiation must be known. This, in turn, requires that atmospheric parameters affecting radiative transfer be determined. Optical depth, temperature, pressure, and relative humidity are measured on site throughout the morning of the Landsat overpass. It is not feasible, however, to measure all the necessary parameters. For example, the verticle structure of the atmosphere, and aerosol properties, such as refractive index, are not easily determined. These unknowns must be characterized with assumed values, based upon data reported in the literature and published models of the atmosphere.

Various models have been constructed which define properties such as temperature, pressure, density, and ozone and water vapor concentrations, as a function of altitude. The U.S. Standard Atmosphere of 1962 (USSA, 1962; Valley, 1965) was established jointly by the U.S. Air Force, U.S. Weather Bureau, and NASA. It gives mean annual values for the midlatitude belt. To account for variations with latitude and season, the U.S. Standard Atmosphere Supplements of 1966 (USSAS, 1966) were established. McClatchey, et al. (1972; 1978) makes use of these data to construct an attenuation model for the atmosphere. This work is the basis of the LOWTRAN 6 (Kneizys, et. al., 1983) computer code.

In addition to knowing the atmospheric properties for days in which Landsat images the earth over White Sands, it is convenient to know what range these parameters may assume. This allows us to define measurement techniques, and to estimate the uncertainty of the calibration procedure. This chapter defines a set of model parameters, applicable to the White Sands area. These are summarized in the final table of the chapter, Table 4.9. Particular attention is given to those parameters which are required as input to the Herman Code. In addition, the range these parameters may assume is predicted. These data are used in the sensitivity study, Chapter 5, and were also used in Chapter 1 to predict the saturation of Landsat imagery. We begin by discussing aerosol characteristics.

Aerosol Characteristics

An aerosol is a dispersed system of small particles suspended in a gas. The aerosols which are present in the earth's atmosphere have a variety of origins. These include dusts (particularly from arid zones and deserts), volcanic ash, foliage exudations, sea salts, and combustion products. Aerosols introduced into the atmosphere are modified by coagulation, fallout, and washout. The number of very large and very small particles tend to decrease, leaving most particles in the 0.01-10.0 μm range. The exact composition of these aerosols depend upon local sources and sinks, meteorological conditions, and geographical locale. Common atmospheric aerosol materials are a 75% H_2SO_4 solution, water soluble materials consisting of ammonium, calcium sulfate and organic materials, dust, soot, clay, and $(NH_4)_2SO_4$.

To the extent that they can be modeled as isotropic spheres, Mie theory can predict the absorption and scattering of light by aerosols. As input to the Mie equations, however, such aerosol properties as refractive index, radial size distribution, and verticle distribution within the atmosphere are required. Techniques exist which enable us to measure some parameters. One technique is the inversion of optical depth data to obtain the aerosol radial size distribution. The reductions of such measured data are discussed in Chapter 4. Other parameters are more difficult to measure. Consider, for example, the measurement of refractive index. Not only are measurement techniques relatively inaccurate, but several months are often required to collect samples and evaluate their properties. Model data, therefore, are as appropiate as any. The vertical distribution could potentially be determined in-situ, but only through use of costly techniques, such as lidar. As we shall see, the large uncertainly which can be tolerated in this parameter does not warrant such an expensive and time consuming effort. For the most part, therefore, model values for aerosol parameters are assumed.

Radial Size Distributions

One of the most popular models for the radial size distribution is the Junge, or power law distribution (defined by Junge, 1963). This law was developed from measurements made over Germany in 1958. McCartney (1976) references many investigators who have successfully fit their measured data to this function. The Junge distribution is

$$n(r) = \frac{dN}{N\, d(\log r)} = c' r^{-\nu} \quad . \tag{4.1}$$

Here N is the number of particles per unit volume, c' is a normalization

constant, and the exponent ν determines the slope of the distribution curve. Thus, n(r) is the number of particles per increment in log r, normalized to the total number of particles. The integral of the size distribution over the radial limits is defined as unity. By noting that d(log r)=0.434 dr/r, the nonlogarithmic form of the distribution is found:

$$n(r) = dN/(N\,dr) = cr^{-\nu+1} \quad , \tag{4.2}$$

where c=0.434c'. The parameter ν typically ranges from $2.5<\nu<4.0$. It is noted that the relative number of small particles increases with ν. The Junge distribution is depicted in Figure 4.1(a) for this range.

Early on a wavelength dependence to optical depth was empirically related to the radial size distribution of aerosols. The first such relationship was suggested by Angstrom (1929) who concluded

$$\tau_{Mie} = a\lambda^{-\gamma} \quad . \tag{4.3}$$

For small particles $\gamma=4$, thus giving the Rayleigh relationship. Under hazy conditions γ may be less than one. By assuming a Junge distribution, the above relationship can easily be derived, as was done by van de Hulst (1957). Equation (2.56) is first used to describe the Mie component of optical depth in terms of the cross section $\sigma_{Mie}(r)$ and radial size distribution n(r). Making the change of variable $\alpha=2\pi r/\lambda$, and substituting for n(r) from (4.2) we obtain

$$\tau_{Mie} = c(\lambda/2\pi)^{-\nu+2} \int \int N(z)\, \sigma_{Mie}(\alpha)\, \alpha^{-\nu+2}\, d\alpha\, dz \tag{4.4}$$

It is apparent that the exponent γ within (4.3) is related to the Junge size distribution by $\gamma=\nu-2$.

Other commonly used radial size distributions are summarized by Russell et al. (1981), and Yue and Deepak (1983). These include the

lognormal distribution and the modified gamma distribution proposed by Deirmendjian (1983). The lognormal is probably the most popular for background stratospheric aerosol studies. It is presented in Figure 4.1(b), and given by

$$n(r) = \frac{A}{\sqrt{2\pi}\ln\sigma}\ \frac{1}{r}\ \exp\left(-\frac{\ln^2(r/r_g)}{2\ln^2\sigma}\right) \quad . \tag{4.5}$$

Recommended values are σ=1.86 and r_g=0.07 μm, but the latter is often adjusted between 0.03 and 3.0 μm to model different atmospheric conditions.

Since the modified gamma function has four adjustable constants, it is frequently used to fit measured data. It is of the form

$$n(r) = Ar^{\alpha}\exp(-Br^{\gamma}) \quad . \tag{4.6}$$

The name is derived from the gamma distribution, which (4.6) reduces to when γ=1. Deirmendjian (1969) has defined constants for three different haze models. These constants are given in Table 4.1. The constant A, as determined by Deirmendjian, is determined such that the integral of n(r) is equal to 100 particles/cm^3, when integrated from zero to infinity. The constant A' is that required to satisy (2.55). That is, n(r), when integrated between the radial limits, taken here as 0.01 and 10.0 μm, equals one. Model H is used for stratospheric dust particles, model L to represent continental aerosols, and model M is applied to maritime and coastal aerosols. These three size distributions are drawn in Figure 4.1(c). Here, as for the Junge and lognormal curves, the radial limits are taken as 0.01 and 10.0 μm.

It must be kept in mind that no single model can define the radial size distribution precisely, as it is a dynamic property of the

atmosphere. Even on a short time scale, changes in optical properties may result from local fluctuations in temperature and water vapor concentrations. As humidity increases, water vapor may be absorbed by the particle, resulting in an increase of particle size, and also a change in the effective refractive index.

Refractive Index

The complex refractive index of an aerosol particle is dependent on wavelength and the composition of the particle. Table 4.2, from Kent, Yue, and Deepak (1983), lists these refractive indices for common materials. Of particular interest to us, however, are the atmospheric studies made in the southwestern United States. For example, researchers at the U.S. Army Atmospheric Sciences Laboratory, White Sands Missile Range, have collected and analyzed local atmospheric particles. Their intent is to understand the composition and scattering properties of these aerosols.

Lindberg and Gillespie (1977) are one such research team who used a cascade impactor to collect and separate particles into one of eight size bins. After collecting continuously for three months, enough particles were obtained for analysis. To determine composition, a potassium bromide spectroscopy technique was used; the imaginary component of refractive index was determinded from a Cary 14 spectrophotometer. They discovered that particles of a given size range had a distinct composition, hence refractive index. The imaginary component of refractive index was found to vary over several orders of magnitude. A strong wavelength dependence was also noted. The giant particles (> 1 μm) were composed of clay minerals (montmorillonite,

illite, and those of the kaolin group), gypsum, quartz, and calcite. These particles have negligibly small imaginary indices, typically <0.001, throughtout the visible and near infrared. Submicron particles were predominately carbon and weakly absorbing ammonium sulfate. Carbon is known to be a strong absorber, with an imaginary index near 0.5. Lindberg and Gellespie concluded that there is no single value of refractive index that can be used to describe the aerosols over New Mexico.

From data such as these, Jennings, Pinnick, and Auvermann (1978) have proposed a bimodal model of refractive index for aerosols found within the White Sands region. Table 4.3 lists their light aerosol loading model (they also define a model for heavy loading). Typical and extreme values of refractive index are given for two radial modes. At 10.6 μm, minimum extinction is obtained using ammonium sulfate (n=1.99-0.06i) for the small particle mode, and sodium nitrate (n=1.19-0.07) for the large particle mode. The maximum values of extinction are determined from carbon (n=2.02-1.28i) and quartz (n=2.18-0.02i) for the small and large modes, respectively. They note that serious errors are introduced in the computed extinction if an average refractive index values is used.

Using these data as a reference, a value of 1.54-0.01i was chosen as the value with which to model the refractive index of aerosols over White Sands. The sensitivity of calibration to refractive index will be analyzed, using the entire range of refractive index values, as defined in Table 4.3.

Vertical Distribution

Using standard nomenclature, as defined by the International Union of Geodesy and Geophysics in 1960, the atmosphere is divided vertically

into four layers on the basis of temperature. These layers are the troposphere, stratosphere, mesosphere, and the thermosphere. The tops of each layer are respectively called the tropopause, stratopause, mesopause, and thermopause. This stratification of the atmosphere is depicted in Figure 4.2, from McCartney (1976). The troposhere, or layer closest to the earth, contains three-fourths of the earth's air, and nearly all the water vapor and atmospheric particles. On average, the temperature decreases here at a lapse rate of -6.5 °C/km. The tropopause is defined as that altitude where the lapse rate goes to zero. This occurs at approximately 11 km, but varies from greater than 16 km in the tropics (due to warmer air and greater mixing), to less than 9 km in the polar regions. The stratosphere continues next, to about 50 km. Between the tropopause and approximately 20 km, temperatures are constant, near -56 °C. Temperatures then increase in the region of increased ozone, due to an increased absorption of ultraviolet radiation from the sun.

The first 5 km of the atmosphere is a region of strong vertical mixing. This is attributed to factors such as heat transfer across the earth/air interface, winds, and turbulence created by local topography. The size distribution does not change much within this region, but both pressure and particle number density decrease exponentially with altitude. This decrease in particle concentration was measured, by Penndorf (1954), from the study of solar attenuation during eight aircraft flights. His measurements of Mie extinction with altitude were fit to an equation of the form

$$\beta_{Mie}(z,\lambda,V) = \beta_{Mie}(0,\lambda,V)\ \exp(-z/H_p) \quad , \qquad (4.7)$$

where $\beta_{Mie}(0,\lambda,V)$ is the extinction at ground level, and the scale height,

H_p, was found to vary from 1 to 1.4 km. The latter parameter was defined as having a representative average of H_p=1.2 km. Recalling that extinction is related to particle number density through the cross section, assumed constant with altitude, particle concentration is also found to obey an exponential falloff, expressed in terms of the same scale height H_p.

A more generalized and often quoted model of the vertical distribution of aerosols is that given by Elterman (1968). This distribution is defined from an average profile measured under clear atmospheric conditions (estimated to be 23 km in visibility). The experimental set-up is described in Elterman (1966). An intensity modulated searchlight beam was projected into the sky over White Sands, New Mexico. This site was at an elevation of 1.39 km. Synchronous detection at λ=0.55 μm was made 30.2 km away, from Sacramento Peak. Scattering data were obtained to 35 km altitude, at 1 km resolution. It was possible to obtain data to greater altitudes, but aerosol attenuation was considered negligible, and therefore not of interest in this region.

One hundred, nineteen extinction profiles were acquired from December 1963 to April 1965. Of these, the latter 79 were averaged to obtain the vertical profile model. Earlier data were deleted so as to avoid including the unusually high values of stratospheric dust which were present as a result of the Mt. Agung volcanic eruption, March 1963. The Penndorf model was next used to extend the model from 3.7 km to sea level. Finally, a least square fit on data from 26 to 32 km was made, thus enabling the model to be extended to 50 km. This extinction model for aerosol scatterers is presented in Table 4.4, along with a molecular

number density profile versus altitude. The latter is defined by the USSA (1962). These profiles, along with the ozone and water vapor profiles to be discussed later, are normalized and used within the Herman Code. Here, the optical depth components are computed as a function of altitude, given optical depths at ground level. If the Elterman model of Mie extinction versus altitude is divided by the aerosol cross section at 0.55 μm, a number density profile can be obtained.

The Elterman data confirm the existence of a stratospheric dust layer at 20 km. This layer, observed by many other researchers, is a stable region of sulfate particles and sulfuric acid droplets. It is found over both urban and rural regions, and exists at an altitude approximately equal to that of greatest ozone concentration. In this region the smaller particles rapidly decrease with altitude. Those of radius less than 0.1 μm are nonexistant near 20 km. The size distribution of larger particles, however, does not change greatly over that at lower altitudes.

Visibility

In order to model aerosol optical depths under a variety of atmospheric conditions, Elterman (1970) used visibility to compute atmospheric extinction at sea level. Visibility, V, or meteorological range, is defined, under sunlit conditions, as the greatest horizontal distance at which an observer, at ground level, can distinguish a black object against the background sky. It is thus a subjective evaluation of the attenuation of contrast. As an observer looks along a horizontal path, contrast is reduced due to direct sunlight, diffuse skylight, and ground reflected light scattered towards the observer. The observed

contrast of an ideally black object, at distance V, is given as

$$C = -\exp(-\beta_{ext} V) \tag{4.8}$$

(a negative number, as the object is darker than the background, and as contrast is defined as the object minus background, divided by background radiance). Taking the visual threshold of perception as C=0.02 (the lowest contrast at which an object can just be distinguished), extinction is determined as a function of visibility:

$$\beta_{Mie}(0,0.55,V) = 3.912/V - \beta_{Ray}(0.55) \tag{4.9}$$

This expression was derived by noting $-\ln(0.02)=3.912$, and setting $\beta_{ext}=\beta_{Mie}+\beta_{Ray}$. The latter can be justified by assuming absorption over distances on the order of the visual range V are negligible. The extinction that is defined in this manner is for a wavelength of 0.55 μm, the wavelength at which the eye is most sensitive, and for an altitude of z=0 km. In practice, measuring visual range is an imprecise science, relying on the subjective opinion of the observer, and requiring the presence of an object at a distance just equal to that at the extreme of visual perception. Nevertheless, it is useful in computing a model of optical depth τ_{Mie}, as is discussed next.

For altitudes above the mixing layer, taken as 5 km, Mie extinction is assumed independent of ground conditions, hence visibility. At a wavelength of 0.55 μm this extinction is modeled by the data presented in Table 4.4. Conversely, at ground level extinction is determined directly from visibility, via Equation (4.9). For intermediate altitudes a scale height is computed to fit these boundary conditions. That is, from Equation (4.7)

$$H_p = z/\ln[\beta_{Mie}(0,0.55,V)/\beta_{Mie}(z,0.55)] \tag{4.10}$$

where

$z = 5$ km

$\beta_{Mie}(0,0.55,V) = 3.912/V - \beta_{Ray}(0.55)$

$\beta_{Ray}(0.55) = 1.162E{-}02\ km^{-1}$

$\beta_{Mie}(5,0.55) = 5.02E{-}03\ km^{-1}$.

After solving for scale height, Mie extinction is determined for all altitudes below 5 km through use of Equation (4.7), and above this altitude through the measured Elterman data, Table 4.4.

Using the above, the Mie optical depth at a wavelength of 0.55 μm is easily computed by integrating Mie extinction over all altitudes:

$$\tau_{Mie}(0.55,V) = \int_0^5 \beta_{Mie}(0, .55,V)\ \exp(-z/H_p)\ dz + \int_5^\infty \beta_{Mie}(z,0.55)\ dz \tag{4.11}$$

$$= \beta_{Mie}(0,0.55,V)\ H_p(1-\exp(-5/H_p)) + B5INTEG\ .$$

Here the first term is a function of visibility; the second term is the Elterman (1968) data integrated between z=5 km and ∞.

Elterman next scaled this value of optical depth, using the data of Curcio, Knestrich, and Cosden (1961), to determine the spectral distribution of $\tau_{Mie}(\lambda,V)$. Denoting the extinction data reported by these authors as $\beta_c(\lambda)$, the Mie component of optical depth is found for an arbitrary wavelength:

$$\tau_{Mie}(\lambda,V) = \tau_{Mie}(0.55,V)\ \ \beta_c(\lambda)/\beta_c(0.55)\ . \tag{4.12}$$

To justify this the following argument is made. It is noted that the ratio of Mie cross sections (integrated over the normalized radial size distribution), $\sigma_{Mie}(\lambda)/\sigma_{Mie}(0.55\ \mu m)$, is independent of visibility.

Extinction is related to meteorological conditions only through the number density, or $\beta_{Mie}(z,\lambda,V)=N_{Mie}(z,V)\ \sigma_{Mie}(\lambda)$. (This is an approximation, ignoring changes in radial size distribution and refractive index.) Thus,

$$\beta_{Mie}(0,\lambda,V) = \beta_{Mie}(0,0.55,V)\ \sigma_{Mie}(\lambda)/\sigma_{Mie}(0.55) \qquad (4.13)$$

$$= \beta_{Mie}(0,0.55,V)\ \beta_c(\lambda)/\beta_c(0.55)$$

That is, Mie extinction, at ground level and at a chosen wavelength, is determined from the product of extinction at λ=0.55 μm with the ratioed Curcio data, $\beta_c(\lambda)/\beta_c(0.55\ \mu m)$. As before, Mie optical depth is determined from the integration of extinction with altitude. As extinction for the new wavelength scales as $\beta_c(\lambda)/\beta_c(0.55)$, a constant independent of altitude, so does optical depth.

In selecting a model of τ_{Mie} for the White Sands area, Elterman's model was selected for 0.55 μm. Angstrom's formula was then used, rather than the Curcio data, to determine τ_{Mie} at other wavelengths. Hence, after determining $\tau_{Mie}(0.55,V)$ from Equation (4.11), other spectral τ_{Mie} values were determined via

$$\tau_{Mie}(\lambda,V) = \tau_{Mie}(0.55,V)\ (\lambda/0.55)^{-\nu+2} \ . \qquad (4.14)$$

To model clear air conditions, a visibility of 100 km, and ν=2.5, have been chosen for the standard model. The resulting τ_{Mie} values are summarized in Table 4.9.

Molecular Absorbers

In the visible and near infrared wavelengths water vapor, oxygen, and carbon dioxide are the primary atmospheric gases which produce strong absorption lines. Figure 4.4 shows how each of these contribute to atmospheric absorption for a vertical path. The extent of the Thematic Mapper (TM) bands are also given. From this figure it is apparent that

ozone and water vapor are the primary absorbers whose effects will have to be accounted for in the calibration process. For this reason, this section focuses on these two gases. Water vapor absorption becomes significant for wavelengths greater than 0.70 μm; carbon dioxide has absorption bands which overlap TM bands 5 and 7. In addition to these, there is significant ozone absorption from 0.4 to 0.9 μm, with a maximum near 0.6 μm. This is due to the Chappius bands, a term applied to this ozone continuum. Nitrogen dioxide also has continuum absorption from approximately 0.34 to 0.50 μm, with a maximum near 0.41 μm. The magnitude of NO_2 absorption is small, and is ignored here.

Ozone

Ozone is a minor constituent, but principal absorber of solar radiation, responsible for the depletion of solar radiation between 0.2 and 0.3 μm. It is primarly created between altitudes of 20 and 30 km, where large numbers of oxygen molecules are dissociated by the absorption of ultraviolet radiation. The predicted columnar ozone content of the atmosphere is dependent on both season and latitude, as is shown in Figure 4.5, from London (1962). Here, the average atmospheric content is plotted for four seasons as a function of latitude. An annual average is also defined, again dependent upon latitude. The total amount of ozone is a maximum in spring and a minimum in autumn, with the largest amplitude of variation at high latitudes. For latitudes north of the tropic zone, seasonal variations are nearly sinusoidal. Measurements made over Tucson (King and Byrne, 1976) show that ozone can be expressed as

$$N_{oz} = (255.3 \pm 4.0 \text{ matm-cm}) + (42.6 \pm 5.0 \text{ matm-cm}) \sin(2\pi x - \phi) \quad (4.15)$$

where x is the fractional time of year. The maximum occurs about 23

April, the minimum about 23 October. As White Sands is roughly at the same latitude, this dependence is assumed an appropriate model for our test site.

The total ozone content of a vertical column of air is usually expressed in units of $(matm\text{-}cm)_{STP}$. With an atmospheric ozone content of N_{oz} atm-cm, where 1 atm-cm=10^{-3} matm-cm, there would be N_{oz} cm in height of pure absorber contained in a square centimeter at standard pressure (1013.25 mb) and temperature (273.15 K). Also, 1 atm-cm=2.69×10^{19} molecules/cm, independent of the absorbing gas. Table 4.5 gives one model for the vertical distribution of ozone within the atmosphere. This particular profile is the low latitude profile measured under conditions in which the total ozone content was approximately 250 matm-cm. It has been selected, from those defined by Mateer, DeLuisi, and Porco (1980), as being the most appropiate with which to model White Sands. The original source of these data include ozonesonde data archived by the World Ozone Data Centre, and that from the USAF ozonesonde network operated during the early 1960's. In Table 4.5, ozone content is defined for 34 atmospheric layers, where the atmospheric pressure at the base of a layer is $\sqrt{2}$ times the atmospheric pressure at the top of the layer. The base of the lowest layer is taken to be 1013.25 mbar, standard pressure.

The spectral dependence of ozone absorption is usually taken as that from Vigroux (1953). These data are based upon laboratory measurements, taken at 1013 mbar and 15°C. These absorption coefficients, as published in Elterman (1968), are listed in Table 4.6. To precict an optical depth for a given time of year the product of number density, such as modeled by Equations (4.15), and a spectral coefficient,

as interpolated from Table 4.6, is determined

$$\tau_{oz}(0,\lambda) = N_{oz}(0)\ \sigma_{oz}(\lambda) \qquad (4.16)$$

To compute the optical depth from measured parameters for a given wavelength and altitude

$$\tau_{oz}(z,\lambda) = \tau_{oz}(0,\lambda_r)\ \frac{\sigma_{oz}(\lambda)}{\sigma_{oz}(\lambda_r)}\ \frac{N_{oz}(z)}{N_{oz}(0)}\ . \qquad (4.17)$$

The parameter $\tau_{oz}(0,\lambda_r)$ is that component of optical depth which is deduced from Langley plot measurements, at a radiometer wavelength of λ_r and at ground elevation, z=0 km. The ratios $\sigma_{oz}(\lambda)/\sigma_{oz}(\lambda_r)$ and $N_{oz}(z)/N_{oz}(0)$ are determined from Tables 4.6 and 4.5, respectively.

Water Vapor

The amount of water vapor that the atmosphere can contain depends on the air temperature. Below -40°C this amount is negligible. To quantify just how much is present, one of many functions of pressure, temperature, or density is used. Absolute humidity is defined by the actual partial pressure in millibars, or by the actual vapor density in gms/m³. Vapor pressure and density are related by $P=\rho RT$, where R is the specific gas constant of the gas in question (universal gas constant divided by the molecular weight of the gas). For water vapor R=461.5 J/kg K, while for dry air R=287.06 J/kg K. Relative humidity is the ratio of actual vapor pressure, at a stated temperature, to the saturation value at that temperature. Other common units are mixing ratio and precipitable water. The mixing ratio is the mass of vapor contained in a unit mass of dry air. It is sometimes expressed in units of grams per kilogram. Precipitable water is the amount of water contained in a vertical air column of unit cross section.

The temperature measures of water vapor are the dew point, T_d, and frost point, T_f, temperatures. Dew point temperature is the temperature at which a given parcel of air would have to be cooled to reach saturation. Frost point temperature is defined in the same way, except that saturation is with respect to ice.

In modeling the sensitivity of water vapor to the calibration process, variations in absorption will be referred to in terms of water vapor density at ground level. The anticipated range of water vapor is determined from the expected range of late morning temperatures for the area. Figure 4.6, from McClatchey (1972), is used to convert these temperatures, at a given relative humidity, to water density, at sea level. From a temperature 10°F, and low humidity, to 70°F, high humidity, water vapor varies from approximately 0.01 to 1.0 gm/cm² km. The verticle profile of water vapor is modeled after data from Sissenwine, Grantham, and Salmela (1968). These data, presented in Table 4.7, assume a density of 0.59 gm/cm² km at ground level (corresponding to a temperature of 15°C and relative humidity of approximately 50%), and 1.417 gm/cm² for the integrated amount of water vapor throughout the atmosphere (as water vapor falls off exponentially, a scale height was defined for each layer, then each layer was integrated over this exponential distribution).

At the test site, relative humidity is usually measured by a psychrometer. This consists of two thermometers, one of which is covered and saturated with water. As water evaporates, the temperature of the wet bulb decreases. The difference in temperatures is a measure of the relative humidity. When radiosonde measurements are made, an electrical

hygrometer is used. The hygrometer relies on the change in state of a material with moisture. A polystyrene slide, coated with a thin layer of a hydroxyethyl cellulose, is constructed with electrodes on either side. The electrical resistivity of the coating increases as the humidity increases.

Within the Herman code, it is not the actual water vapor that is of interest, but the transmittance, T, at a given wavelength. This is expressed in terms of τ_{H2O} for water vapor (recall $T=\exp(-\tau)$). To model transmittance for atmospheric gases, the LOWTRAN 6 computer code was run. After integration between the equivalent TM bandpasses, as computed by Palmer (1984), an average τ_{H2O} value was determined for TM bands 4,5, and 7. These were found to be 0.0335, 0.0915, and 0.0594, respectively. (The corresponding values which characterize carbon dioxide absorption were τ_{CO2}=0.0, 0.0094, and 0.0035.) The range of predicted τ_{H2O} values for White Sands were computed by scaling these τ_{H2O} values by the ratio $\rho_{H2O}(0,RH,T)/0.59$, where the water content at White Sands may vary between $\rho_{H2O}(0,RH,T)$=0.01 and 1. gm/cm^2. The resulting τ_{H2O} values are summarized in Table 4.9.

Currently, the amount of water vapor present within the atmosphere, for days of the Landsat overpass, is determined from measured relative humidity, temperature, and Figure 4.6. It is hoped that within the near future this technique will be replaced by a direct measurement of τ, made with filters matched to TM bands 5 and 7. This will be done with the solar radiometer and Langley plot technique, thereby removing many uncertainties associated with use of LOWTRAN transmittance spectra and the scaling technique.

Solar Irradiance

To compute the spectral radiance incident on an in-orbit sensor, the exo-atmospheric solar spectral irradiance must be known to a high level of certainty. This quantity is defined as the irradiance one astronomical unit from the sun, within a specified wavelength interval, striking a unit surface in free space perpendicular to the sun's rays (having units such as W/cm^2 μm). It is possible to measure this parameter directly by using a solar spectral radiometer. The irradiance data, when extrapolated to zero airmass, yield values for the spectral exo-atmospheric irradiance. This, the Langley plot technique, is discussed in Chapter 4. To rely on such data, the radiometer must be calibrated to an acceptable absolute accuracy, if possible to the 1% level. In addition, a temporally stable atmosphere is required. Because of these constraints, we have chosen to rely on published data. It is felt that these data are of greater accuracy than we can presently measure at White Sands.

Published solar irradiance data are corrected for varying earth-sun distance by normalization to a mean earth-sun distance of one astronomical unit, where 1 AU = 1.496 x10^8 km. Variations of this distance throughout the year result in variations of solar irradiance by as much as 6.7%. The minimum earth-sun distance is about 0.98327 AU, occuring about January 3. The maximum distance of 1.01673 AU occurs about July 4. Ephemeris tables, such as the American Ephemeris and Nautical Almanac (yearly), can be consulted for the exact distance for a given day of the year. Conversely, mathematical expressions exist from which this distance can be computed. For example, an expression developed by Spencer (1971) gives the eccentricity of the earth's orbit to

an error of less that 0.0001. This expression is

$$(r_0/r)^2 = 1.000110 + 0.34221 \cos \Gamma + 0.001280 \sin \Gamma$$

$$+ 0.000719 \cos 2\Gamma + 0.000077 \sin 2\Gamma \quad . \tag{4.18}$$

The parameter Γ is called the day angle. It has units of radians, given by

$$\Gamma = 2\pi(d-1)/365 \tag{4.19}$$

where d is the day number of the year (d=1 on January 1; d=365 for December 31).

The variability of exo-atmospheric solar spectral irradiance, after normalization to 1 AU, has been measured by Shaw (1982). Using a silicon photodiode, calibrated by reference to an absolute electrical cavity radiometer, he measured the solar spectrum to within 2%, and to a relative calibration of 0.2%. He reported that spectral irradiance at any given wavelength fluctuated by no more that 0.5% from February 1980, to February 1981.

Several solar irradiance data sets have been reported. The work of Neckel and Labs (1981) is the most detailed. They report a mean error of 1.5% in the uv, and 1% in the visible. These data are based upon measurements made early in the 1960's, in Switzerland, at an altitude of 3.6 km (11,800 ft.). The calculation of determining mean disk irradiance, based upon disk center measurements, has been revised for the 1981 publication. In 1974, the American Society for Testing and Materials accepted the data reported by Thekaekara, Kruger, and Duncan (1969) as their recommended engineering standard. These data are often referred to as the NASA/ASTM standard. They were obtained from measurements carried

out by NASA, in 1968-1971, onboard a Convair research aircraft, and are thought to be accurate only to within 5%.

Currently, the data recommended by Frohlich and Wehrli (1981), as published by Iqbal (1983), are used in our Landsat calibration program. They are presented here, within Table 4.8. Values, such as those published by Neckel and Labs, Thekaekara, Arvesen, and others, were combined. They were then adjusted to an integrated value of 1367 W/m^2, the solar contant as proposed by the World Radiation Center (WRC). The World Meteorological Organization adopted this spectrum as the best available, in 1981. It is referred to as the WRC standard.

The solar constant defines the total amount of irradiance from the sun that falls at the top of the earth's atmosphere, at its mean distance from the sun. It is the value of spectral irradiance, integrated over all wavelengths, and measured in units such as W/m^2. The solar output can be approximated by treating the sun as a blackbody with peak spectral exitance near 0.5 μm, corresponding to a 6000 K blackbody curve. In actuality, the effective temperature of the sun is wavelength dependent (Slater, 1980), and the true spectrum is by no means smooth at high spectral resolution because of Fraunhofer absorption lines.

The solar constant can be determined with greater certainty than spectral irradiance values. For high accuracy, measurements from high altitude or from orbit are invaluable, since atmospheric attenuation cannot be exactly corrected for. The actual solar constant seems to fluctuate slightly, but only by a few tenths of a percent over many years. The Solar Maximum Mission satellite measured solar variability to be no larger than 0.2%, although the average solar variability was 0.05%.

The NASA value of the solar constant, adopted in 1971 as their design standard, is 1353 $W/m^2 \pm 21$. The WRC standard differs from the NASA value by only 1%, being 1367 W/m^2 ±1.6. The latter value of the solar constant has been defined by Frohlich (1981), and is based upon data recorded between 1969 to 1980. It accounts for many changes in the state of the art. For example, only since 1975 has it been known that some instrument characteristics are different in the vacuum of space, as compared to terrestrial characteristics. Furthermore, recent measurements employ more accurate cavity-type absolute instruments.

REFERENCES

"American Ephemeris and Nautical Almanac." U.S. Government Printing Office, Washington D.C.

Angstrom, Anders (1929). "On the atmospheric transmission of sun radiation and on dust in the air." Geogr. Ann., Stockholm, 11, 156-166.

Chandrasekhar, S. (1950). Radiative Transfer. Oxford University Press, New York. Also Dover Publications, New York (1960).

Curcio, J.S., G.L. Knestrick, and T.H. Cosden (1961). Atmospheric Scattering in the Visible and Infrared. NRL Report 5567, U.S. Naval Research Laboratory, Washington, D.C.

Dave, J.V. (1969). "Scattering of electromagnetic radiation by a large, absorbing sphere." IBM J. Res. Develop., May, p. 302.

Deirmendjian, D. (1963). "Scattering and polarization properties of polydispersed suspensions with partial absorption." In Electromagnetic Scattering, M. Kerker, ed., Macmillan, New York.

Deirmendjian, D. (1969). Electromagnetic Scattering on Spherical Polydispersions. American Elsevier, New York.

Edlen, B. (1953). "The dispersion of standard air." J. Opt. Soc. Am., 43, p. 339.

Elterman, L. (1966). "Aerosol measurements in the troposphere and stratosphere." Appl. Opt. 5, 1769.

Elterman, Louis (1968). UV, Visible, and IR Attenuation for Altitudes to 50 km. Report AFCRL-68-0153, Air Force Cambridge Research Laboratories, Bedford, Mass., pp. 49.

Elterman, Louis (1970). Vertical-Attenuation Model with Eight Surface Meteorlogical Ranges 2 to 13 Kilometers. Report AFRCL-70-0200, Air Force Cambridge Research Laboratories, Bedford, Mass., pp. 55.

Gucker, F.T., and S. Basu (1953). Right-Angle Molecular Light Scattering from Gases. University of Indiana, Bloomington, Ind., Scientific Report No. 1, Contract AF 10(122)-400.

Frohlich, C. and C. Wehrli (1981). Spectral Distribution of Solar Irradiance from 25000 nm to 250 nm. World Radiation Center, Davos, Switzerland, private communication with M. Iqbal.

Jennings, S.G., R.G. Pinnick, H.J. and H.J. Auvermann (1978). "Effects of particulate complex refractive index and particle size distribution variations on atmospheric extinction and absorption for visible through middle ir wavelengths." Appl. Opt. 17, 3922.

Grams, Gerald W., and James M. Rosen (1978). "Instrumentation for in-situ measurements of the optical properties of stratospheric aerosol particles". Atmos. Tech. 9, Spring.

Junge, C.E. (1963). Air Chemistry and Radioactivity. Academic Press, New York.

Kent, G.S, Glenn K. Yue, and Adarsh Deepak (1983). "Modeling atmospheric aerosol backscatter at CO laser wavelengths. 1: Aerosol properties, modeling techniques, and associated problems." Appl. Opt. 22, 1655.

Kiang, Richard (1983). Sigma Data Corporation, New York. Private communication with Phil Slater.

King, Michael D., and Dale M. Byrne (1976). "A method for inferring total ozone content from the spectral variation of total optical depth obtained with a solar radiometer." J. Atmos. Sci. 33, 2242.

Herman, Benjamin M. (1963). A Numerical Solution to the Equation of Radiative Transfer for Particles in the Mie Region. Ph.D. dissertation, University of Arizona, pp. 130.

Herman, Benjamin M., and Samuel R. Browning (1965). "A numerical solution to the equation of radiative transfer." J. Atmos. Sci., 22, pp. 559-566.

Herman, Benjamin M., Samuel R. Browning, and Robert J. Curran (1971). "The effect of atmospheric aerosols on scattered sunlight." J. Atmos. Sci., 28, pp. 419-428.

Herman, Benjamin M., Anthony J. LaRocca, and Robert E. Turner (1978). "Atmospheric Scattering." In The Infrared Handbook, William L. Wolfe and George J. Zissis, eds., Environmental Research Institute of Michigan, Ch. 4, pp. 76.

Iqbal, Muhammad (1983). An Introduction to Solar Radiation. Academic Press, New York.

Kneizys, F.X., E.P. Shettle, W.O. Gallery, J.H. Chetwynd, Jr., L.W. Abreu, J.E.A. Selby, S.A. Clough, and R.W. Fenn (1983). Atmospheric Transmittance/Radiance: Computer Code LOWTRAN 6. Report AFGL-TR-83-0187, AFRCL, Bedford, Mass., August, pp. 200.

LaRocca, Anthony J. (1978). "Atmospheric absorption." In The Infrared Handbook, William L. Wolfe and George J. Zissis, eds., Environmental Research Institute of Michigan, Ch. 5, pp. 132.

Lindberg, James D., and James B. Gillespie (1977). "Relationship between particle size and imaginary refractive index in atmospheric dust." Appl. Opt. 16, 2628.

Liou, Kuo-Nan (1980). An Introduction to Atmospheric Radiation. Academic Press, New York, pp. 392.

London, J. (1962). "The distribution of total ozone over the northern hemisphere." Sun Work 7, pp. 11-12.

Mateer, Carlton L., John J. DeLuisi, Carolyn C. Porco (1980). The Short Umkehr Method, Part I: Standard Ozone Profiles for use in the Estimation of Ozone Profiles by the Inversion of Short Umkehr Observations. NOAA Technical Memorandum ERL ARL-86, July.

McCartney, Earl J. (1976). Optics of the Atmosphere. John Wiley & Sons, New York, pp. 408.

McClatchey, Robert A., Robert W. Fenn, John E. A. Selby, Frederic E. Volz, and John S. Garing (1972). "Optical Properties of the Atmosphere (Third Edition)." AFCRL-72-0497, August.

McClatchey, Robert A., Robert W. Fenn, John E. A. Selby, Frederic E. Volz, and John S. Garing (1978). "Optical Properties of the Atmosphere." In Handbook of Optics, Walter G. Driscoll, ed., McGraw-Hill, New York, Ch. 14, pp. 65.

Mie, G. (1908). "A contribution to the optics of turbid media, especially colloidal metallic suspensions." Ann. Phys., 25(4), 377-445. In German.

Neckel, H. and D. Labs (1981). "Improved data of solar spectral irradiance from 0.33 to 1.25 m." Solar Phys. 74, 231.

Palmer, James M. (1984). "Effective Bandwidths for LANDSAT-4 and LANDSAT-D' Multispectral Scanner and Thematic Mapper Subsystems." IEEE Trans. Geoscience and Remote Sensing GE-22(3), pp. 336-338, May.

Penndorf, R. (1954). The Vertical Distribution of Mie Particles in the Troposphere. Report AFCRC-54-5, AFCRL, Bedford, Mass.

Russell, P.B., T.J. Swissler, M.P. McCormick, W.P. Chu, J.M. Livingston, and T.J. Pepin (1981). "Satellite and correlative measurements of the stratospheric aerosol. I: An optical model for data conversions." J. Atmos. Sci. 38, 1279.

Sekera, Z. (1955). Scattering matrix for spherical particles and its transformation in investigation of skylight polarization, Appendix D. Final Report, Contract AF 19(122)-239, Dept. of Meteorology, University of California, Los Angeles, pp. 68.

Shaw, G.E. (1982). "Solar spectral irradiance and atmospheric transmission at Mauna Loa Observatory." Appl. Opt. 8, 2006.

Sissenwine, N., D.D. Granthah, and H.A. Salmela (1968). Humidity Up to the Mesopause. Rept. AFRCL-68-0550, Air Force Surveys in Geophysics No. 206. AFCRL, Bedford, Mass.

Spencer, J.W. (1971). "Fourier series representation of the position of the sun." Search, 2(5), 172.

Stratton, J.A. (1941). Electromagnetic Theory. McGraw-Hill, New York.

Thekaekara, M.P., R. Kruger. and C.H. Duncan (1969). "Solar measurements from a research aircraft." Appl. Opt. 8, 1713.

van de Hulst, H.C. (1957). Light Scattering by Small Particles. John Wiley & Sons, New York, pp. 470.

USSA (1962). U.S. Standard Atmosphere, 1962. Cat. No. NAS 1.2:At6/962. GPO, Washington, D.C.

USSAS (1966). U.S. Standard Atmosphere Supplements, 1966. Cat. No. NAS 1.2:At6/966/supp. GPO, Washington, D.C.

Valley, Shea L., ed. (1965). Handbook of Geophysics and Space Environments. McGraw-Hill, New York.

Vigroux, E. (1953). "Contributions a l'etude experimentale de l'absorption de l'ozone." Ann. Phys. (Paris) 8, 709.

Yue, Glenn K., and Adarsh Deepak (1983). "Retrieval of stratospheric aerosol size distribution from atmospheric extinction of solar radiation at two wavelengths." Appl. Opt. 22, 1639.

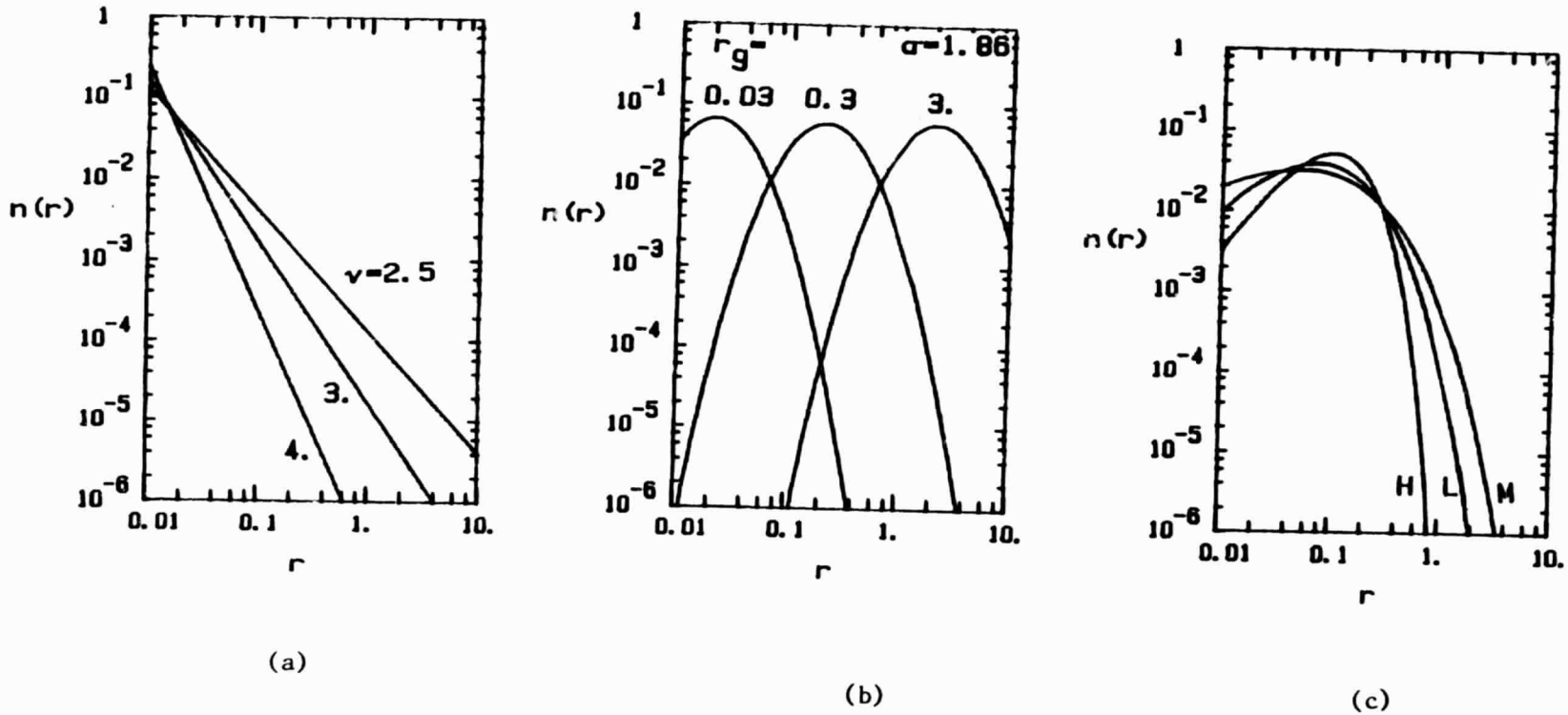

(a) (b) (c)

Figure 4.1 Model radial size distributions. In (a)Junge distribution for ν=2.5, 3.0, and 4.0; (b)lognormal with r_g=0.03,0.3, and 3.0, all with σ=1.86; (c)modified gamma distribution's H, L, and M. All curves are drawn for radial limits 0.01-10.0 μm.

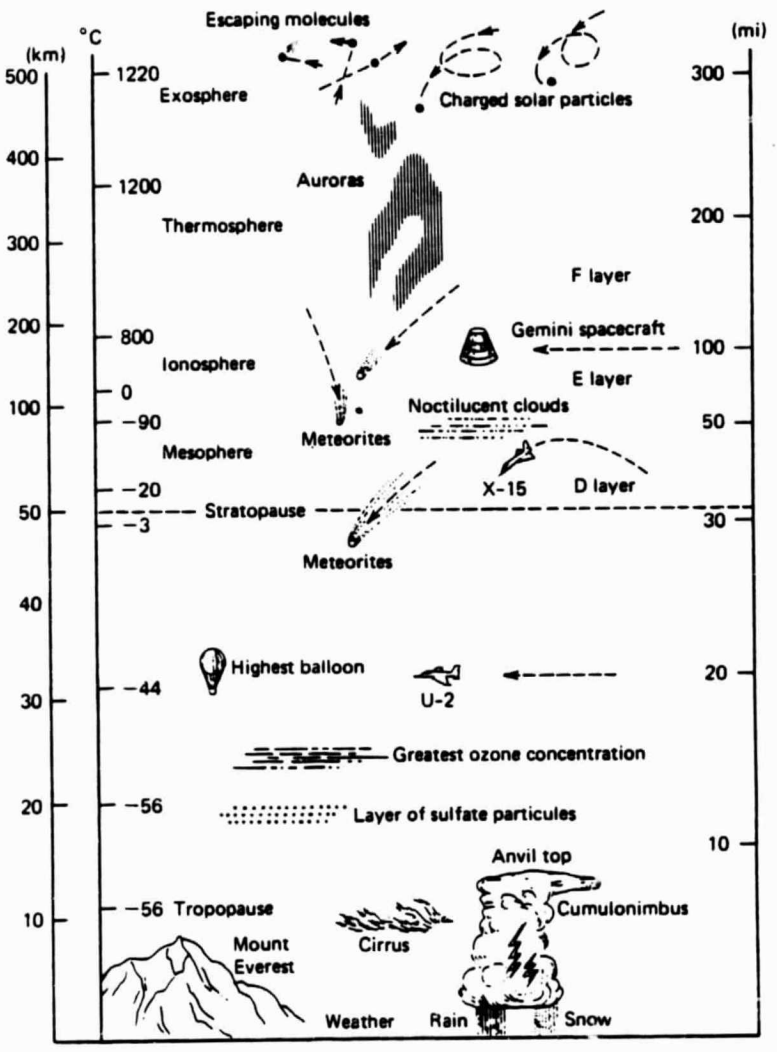

Figure 4.2 Stratification of the atmospheric envelope (from McCartney, 1976).

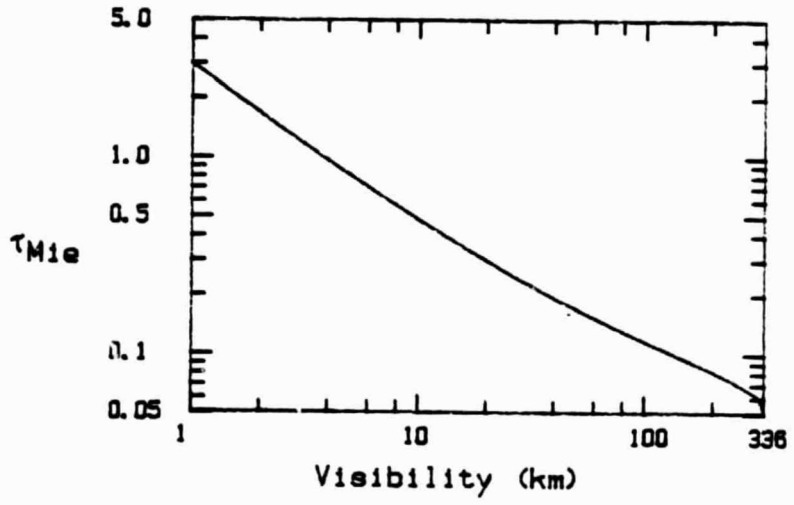

Figure 4.3 Mie optical depth as a function of visibility at a wavelength of 0.55 μm. The haze/clear boundary, as defined by Elterman (1970), is 15 km.

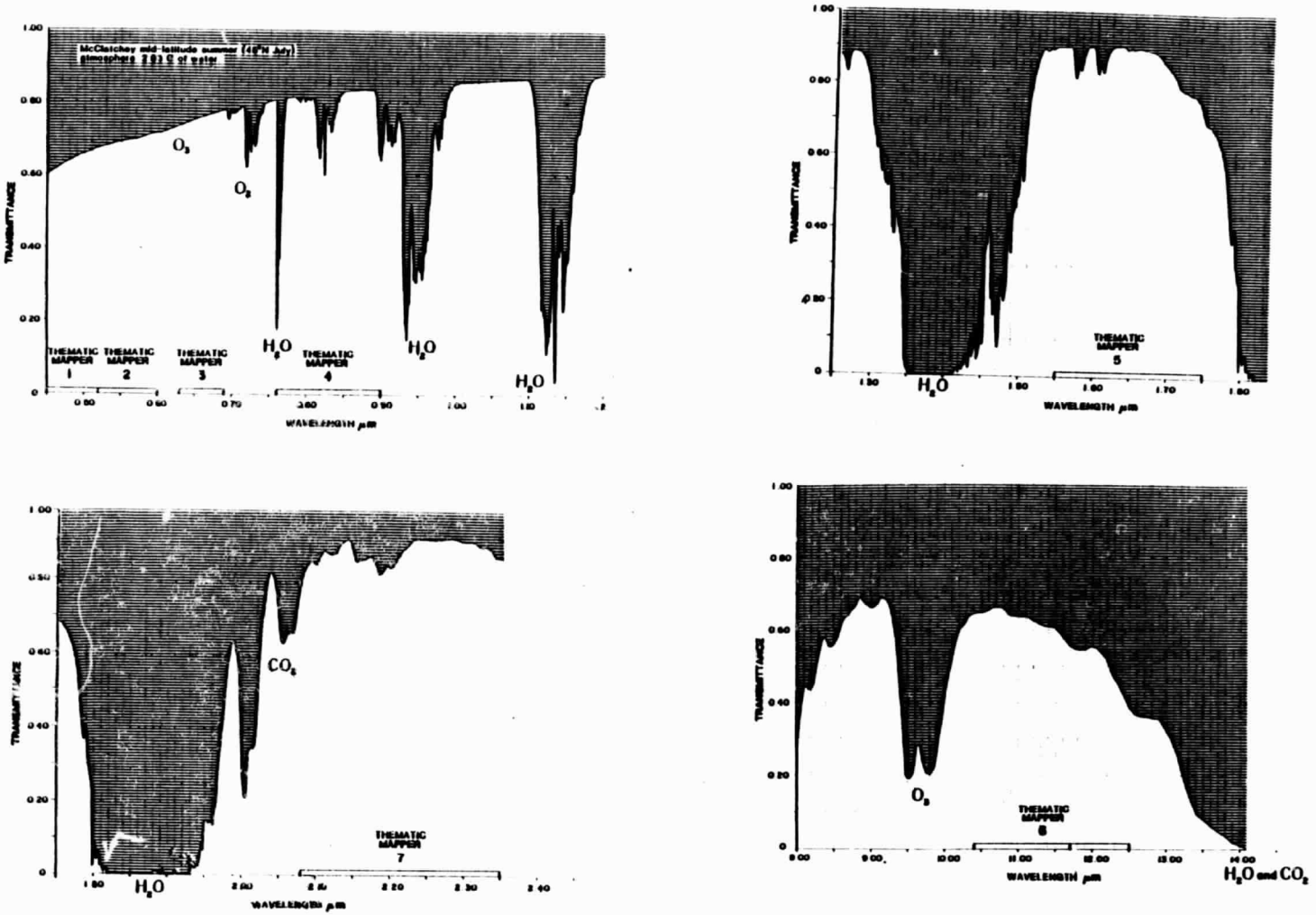

Figure 4.4 Absorption spectra for the principal absorbing gases in the earth's atmosphere (from Kiang, 1983).

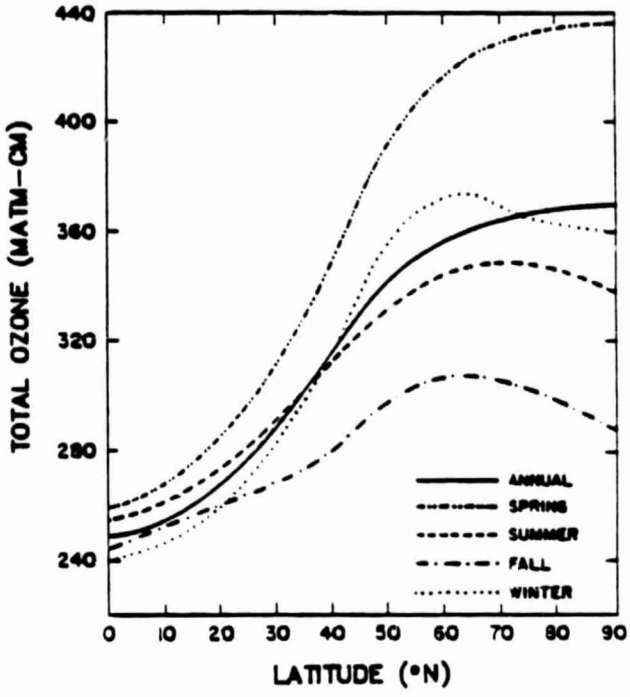

Figure 4.5 Columnar ozone as a function of latitude and season (from London, 1972).

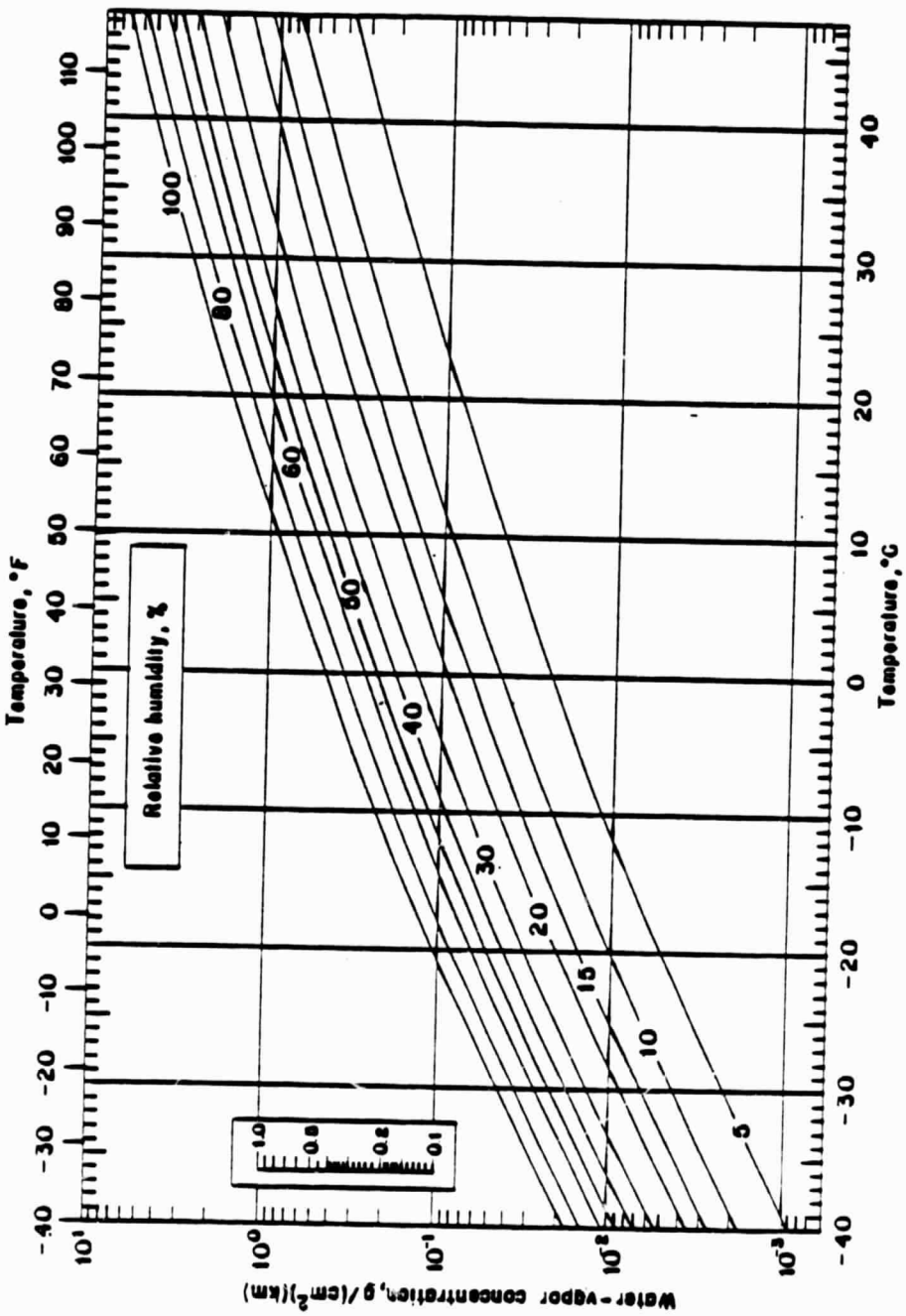

Figure 4.6 Water vapor concentration as a function of temperature and relative humidity (from McClatchey, 1972).

Table 4.1 Haze Model Parameters for the Modified Gamma Distribution

Distribution	A	α	B	γ	A'
Haze M	5.3333E+04	1	8.9443	0.5	4.7115
Haze L	4.9757E+06	2	15.1186	0.5	427.8681
Haze H	4.0000E+05	2	20.0000	1	11572.65

A, α, B, and γ from Deirmendjian (1969). A' defined to normalize n(r), integrated from 0.01 to 10. μm, to unity.

Table 4.2 Refractive Indices of Common Aerosol Materials

Aerosol Models	Complex Index of Refraction, Wavelength (μm) 0.488	0.55	0.6328	1.06
Water	1.336-1.E-09i	1.333-1.96E-09i	1.332-1.5E-08i	1.326-5.E-06i
Maritime	1.418-0.002i	1.418-0.002i	1.415-0.002i	1.405-0.004i
Maritime/Rural	1.475-0.005i	1.474-0.004i	1.473-0.004i	1.463-0.009i
Rural	1.530-0.008i	1.530-0.006i	1.530-0.006i	1.520-0.014i
Rural/Urban	1.569-0.086i	1.569-0.082i	1.569-0.80i	1.560-0.089i
Urban	1.607-0.163i	1.607-0.158i	1.607-0.154i	1.600-0.163i
Water Soluble	1.530-0.005i	1.530-0.006i	1.530-0.006i	1.520-0.017i
Dustlike	1.530-0.008i	1.530-0.008i	1.530-0.008i	1.520-0.008i
Soot	1.750-0.450i	1.750-0.440i	1.750-0.430i	1.750-0.440i
Sea Salt	1.500-2.E-08i	1.500-1.E-08i	1.490-2.E-04i	1.470-2.E-04i
Crystal	1.500-7.E-03i	1.500-6.E-03i	1.490-2.5E-03i	1.470-2.E-03i
75% H_2SO_4	1.432-2.E-08i	1.431-2.E-08	1.429-2.E-08i	1.420-1.5E-06i
Al_2O_3	1.77-2.E-07i	1.77-2.E-07	1.77-2.E-07i	1.76-6.E-08
NaCl	1.55-1.E-07i	1.55-1.E-07i	1.55-1.E-07i	1.53-1.E-07i
$(NH_4)_2SO_4$	1.53-1.E-07i	1.52-1.E-07i	1.52-1.E-07i	1.51-2.4E-06i
Sahara dust				
Volcanic Dust				

From Kent, Yue, and Deepak (1983)

1.66	5.0	10.59
1.316-9.43E-05i	1.325-0.0124i	1.179-0.6777i
1.376-0.004i	1.372-0.010i	1.380-0.057i
1.408-0.010i	1.381-0.012i	1.550-0.071i
1.440-0.016i	1.390-0.013i	1.720-0.085i
1.500-0.096i	1.492-0.116i	1.810-0.198i
1.559-0.175i	1.593-0.218i	1.895-0.310i
1.487-2.E-02i	1.450-0.012i	1.760-0.07i
1.367-8.E-03i	1.250-0.016i	1.620-0.120i
1.78-0.469i	1.970-0.600i	2.220-0.730i
1.456-7.E-04i	1.470-0.0025i	1.500-0.014i
1.456-2.5E-03	1.470-0.02i	1.500-0.2i
1.398-2.72E-04i	1.359-0.0123i	1.737-0.273i
1.74-5.5E-08i	1.62-3.1E-05i	0.55-0.061i
1.53-1.E-07i	1.515E-07i	1.49-1.E-07i
1.49-1.8E-04i	1.46-0.006i	1.98-0.06i
	1.56-0.015i	1.74-0.40i
	1.56-0.009i	1.95-0.40i

Table 4.3 Values of Complex Refractive Indices for a Bimodal Particle Size Distribution Characteristic of Light Desert Aerosol Loading

		Light Aerosol Loading			
		Small Particle Mode		Large Particle Mode	
Wavelength (μm)		Real Index of Refraction	Imaginary Index of Refraction	Real Index of Refraction	Imaginary Index of Refraction
0.55	Minimum	1.52	0.01	1.52	0.0001
	Typical	1.54	0.015	1.54	0.003
	Maximum	1.6	0.03	1.6	0.005
1.06	Minimum	1.5	0.01	1.5	0.0001
	Typical	1.54	0.015	1.5	0.001
	Maximum	1.6	0.06	1.6	0.005
3.8	Minimum	1.56	0.02	1.25	0.001
	Typical	1.6	0.2	1.5	0.02
	Maximum	2.23	1.07	0.86	1.44
10.6	Minimum	1.99	0.06	1.19	0.07
	Typical	2.2	1.25	1.7	0.2
	Maximum	2.04	1.28	2.01	0.02

From Jennings, Pinnick, and Auvermann (1978).

Table 4.4 Model Parameters of Mie Extinction and Molecular Number Density as a Function of Altitude

z (km)	β_{Mie} (km^{-1})	N_{Ray} (cm^{-3})	z (cm)	β_{Mie} (km^{-1})	N_{Ray} (cm^{-3})
0	1.58 E-01	2.547 E+19	26	3.62 E-04	7.123 E+17
1	6.95 E-02	2.311	27	2.77	6.092
2	3.00	2.093	28	2.12	5.214
3	1.26	1.891	29	1.63	4.466
4	6.66 E-03	1.704	30	1.25	3.828
5	5.02	1.531	31	9.55 E-05	3.283
6	3.54	1.373	32	7.31	2.818
7	3.29	1.227	33	5.60	2.406
8	3.39	1.093	34	4.29	2.056
9	3.25	9.712 E+18	35	3.29	1.760
10	3.17	8.598	36	2.52	1.509
11	2.97	7.585	37	1.93	1.296
12	3.12	6.486	38	1.48	1.116
13	2.88	5.543	39	1.13	9.620E E+16
14	2.82	4.738	40	8.66 E-06	8.308
15	2.65	4.049	41	6.64	7.187
16	2.52	3.461	42	5.08	.227
17	2.49	2.959	43	3.89	5.404
18	2.41	2.529	44	2.98	4.697
19	2.03	2.162	45	2.28	4.088
20	1.49	1.849	46	1.75	3.564
21	1.08	1.574	47	1.34	3.112
22	8.13 E-04	1.341	48	1.03	2.738
23	6.22	1.144	49	7.86 E-07	2.418
24	4.93	9.760 E+17	50	6.02	2.135
25	4.15	8.335			

From Elterman (1968). All parameters defined at λ=0.55 μm.

Table 4.5 Vertical Distribution of Ozone

Layer	Ozone amount for Standard Low Latitude Profile (matm-cm)
1	3.96 E+00
2	3.47
3	2.93
4	2.41
5	1.80
6	1.78
7	2.50
8	7.11
9	1.74 E+01
10	2.75
11	3.48
12	3.71
13	3.36
14	2.67
15	1.83
16	1.21
17	7.47 E+00
18	4.30
19	2.31
20	1.21
21	6.31 E-01
22	3.30
23	1.72
24	9.00 E-02
25	4.70
26	2.46
27	1.28
28	6.71 E-03
29	3.51
30	1.83
31	9.58 E-04
32	5.01
33	2.62
34	2.86
Total Ozone	250 matm-cm

From Mateer, DeLuisi, and Porco (1980)

Table 4.6 Ozone Absorption as a Function of Wavelength

λ (μm)	α_{oz} (cm^{-1})
0.27	210.
0.28	106.
0.30	101.
0.32	0.898
0.34	0.064
0.36	0.0018
0.38	0.
0.40	0.
0.45	0.0035
0.50	0.0345
0.55	0.092
0.60	0.132
0.65	0.062
0.70	0.023
0.80	0.01
0.90	0.

From Elterman (1968)

Table 4.7 Model Vertical Profiles of Pressure, Temperature, and Water Vapor

	U.S. Standard Atmosphere, 1962			
Ht. (km)	Pressure (mbar)	Temp (K)	Density (g/m^3)	Water Vapor (g/m^3)
0	1.013E+03	288.1	1.225E+03	5.9E+00
1	8.986E+02	281.6	1.111	4.2
2	7.950	275.1	1.007	2.9
3	7.012	268.7	9.093E+02	1.8
4	6.166	262.2	8.193	1.1
5	5.405	255.7	7.364	6.4E-01
6	4.722	249.2	6.601	3.8
7	4.111	242.7	5.900	2.1
8	3.565	236.2	5.258	1.2
9	3.080	229.7	4.671	4.6E-02
10	2.650	223.2	4.135	1.8
11	2.270	216.8	3.648	8.2E-03
12	1.940	216.6	3.119	3.7
13	1.658	216.6	2.666	1.8
14	1.417	216.6	2.279	8.4E-04
15	1.211	216.6	1.948	7.2
16	1.035	216.6	1.665	6.1
17	8.850E+01	216.6	1.423	5.2
18	7.565	216.6	1.216	4.4
19	6.467	216.6	1.040	4.4
20	5.529	216.6	8.891E+01	4.4
21	4.729	217.6	7.572	4.8
22	4.047	218.6	6.451	5.2
23	3.467	219.6	5.500	5.7
24	2.972	220.6	4.694	6.1
25	2.549	221.6	4.008	6.6
30	1.197	226.5	1.841	3.8
35	5.746E+00	236.5	8.463E+00	1.6
40	2.871	250.4	3.996	6.7E-05
45	1.491	264.2	1.966	3.2E-05
50	7.978E-01	270.6	1.027	1.2
70	5.520E-02	219.7	8.754E-02	1.5E-07
100	3.008E-04	210.0	4.989E-04	1.0E-09

Water vapor profile from Sissenwine (1968).

Table 4.8 Extraterrestrial Solar Spectral Irradiance at Mean Sun-Earth Distance (WRC Spectrum)

λ (μm)	E_0 (W/m²μm)	λ (μm)	E_0 (W/m²μm)	λ (μm)	E_0 (W/m²μm)	λ (μm)	E_0 (W/m²μm)
0.250	64.56	0.475	2016.25	0.790	1142.50	1.900	136.01
0.255	91.25	0.480	2055.00	0.800	1144.70	1.950	126.00
0.260	122.50	0.485	1901.26	0.810	1113.00	2.000	118.50
0.265	253.75	0.490	1920.00	0.820	1070.00	2.100	93.00
0.270	275.00	0.495	1965.00	0.830	1041.00	2.200	74.75
0.275	212.50	0.500	1862.25	0.840	1019.99	2.300	63.25
0.280	162.50	0.505	1943.75	0.850	994.00	2.400	56.50
0.285	286.25	0.510	1952.50	0.860	1002.00	2.500	48.25
0.290	535.00	0.515	1835.01	0.870	972.00	2.600	42.00
0.295	560.00	0.520	1802.49	0.880	966.00	2.700	36.50
0.300	527.50	0.525	1894.99	0.890	945.00	2.800	32.00
0.305	557.50	0.530	1947.49	0.900	913.00	2.900	28.00
0.310	602.51	0.535	1926.24	0.910	876.00	3.000	24.75
0.315	705.00	0.540	1857.50	0.920	841.00	3.100	21.75
0.320	747.50	0.545	1895.01	0.930	830.00	3.200	19.75
0.325	782.50	0.550	1902.50	0.940	801.00	3.300	17.25
0.330	997.50	0.555	1885.00	0.950	778.00	3.400	15.75
0.335	906.25	0.560	1840.02	0.960	77..00	3.500	14.00
0.340	960.00	0.565	1850.00	0.970	764.00	3.600	12.75
0.345	877.50	0.570	1817.50	0.980	769.00	3.700	11.50
0.350	955.00	0.575	1848.76	0.990	762.00	3.800	10.50
0.355	1044.99	0.580	1840.00	1.000	743.99	3.900	9.50
0.360	940.00	0.585	1817.50	1.050	665.98	4.000	8.50
0.365	1125.01	0.590	1742.49	1.100	606.04	4.100	7.75
0.370	1165.00	0.595	1785.00	1.150	551.04	4.200	7.00
0.375	1081.25	0.600	1720.00	1.200	497.99	4.300	6.50
0.380	1210.00	0.605	1751.25	1.250	469.99	4.400	6.00
0.385	931.25	0.610	1715.00	1.300	436.99	4.500	5.50
0.390	1200.00	0.620	1715.00	1.350	389.03	4.600	5.00
0.395	1033.74	0.630	1637.50	1.400	354.03	4.700	4.50
0.400	1702.49	0.640	1622.50	1.450	318.99	4.800	4.00
0.405	1643.75	0.650	1597.50	1.500	296.99	4.900	3.75
0.410	1710.00	0.660	1555.00	1.550	273.99	5.000	3.47
0.415	1747.50	0.670	1505.00	1.600	247.02	6.000	1.75
0.420	1747.50	0.680	1472.50	1.650	234.02	7.000	0.95
0.425	1692.51	0.690	1415.02	1.700	215.00	8.000	0.55
0.430	1492.50	0.700	1427.50	1.750	187.00	9.000	0.35
0.435	1761.25	0.710	1402.50	1.800	170.00	10.000	0.20
0.440	1755.02	0.720	1355.00	1.850	149.01	25.00	0.12
0.445	1922.49	0.730	1355.00				
0.450	2099.99	0.740	1300.00				
0.455	2017.51	0.750	1272.52				
0.460	2032.49	0.760	1222.50				
0.465	2000.00	0.770	1187.50				
0.470	1979.99	0.780	1195.00				

From Iqbal (1983)

Table 4.9 Summary of Model Parameters Defined for White Sands Missle Range

TM Band		1	2	3	4	5	7
WAV (micrometers)	0.5500	0.4860	0.5710	0.6610	0.8380	1.6800	2.2200
TMIE (Visibility km/NU)							
(23/ 2.5)	0.2718	0.2891	0.2667	0.2479	0.2202	0.1555	0.1353
(23/ 3.0)	0.2718	0.3075	0.2618	0.2261	0.1784	0.0890	0.0673
(23/ 4.0)	0.2718	0.3480	0.2521	0.1881	0.1171	0.0291	0.0167
(100/ 2.5)	0.1156	0.1230	0.1134	0.1054	0.0936	0.0661	0.0575
(100/ 3.0)	0.1156	0.1308	0.1113	0.0962	0.0759	0.0378	0.0286
(100/ 4.0)	0.1156	0.1480	0.1072	0.0800	0.0498	0.0124	0.0071
(200/ 2.5)	0.0813	0.0865	0.0798	0.0742	0.0659	0.0465	0.0405
(200/ 3.0)	0.0813	0.0921	0.0784	0.0677	0.0534	0.0266	0.0202
(200/ 4.0)	0.0813	0.1042	0.0755	0.0563	0.0350	0.0087	0.0050
TRAY (Pressure mbar)							
(800.00)	0.0776	0.1287	0.0666	0.0368	0.0141	0.0009	0.0003
(900.00)	0.0873	0.1448	0.0749	0.0414	0.0159	0.0010	0.0003
(1000.00)	0.0970	0.1609	0.0833	0.0460	0.0176	0.0011	0.0004
(1013.25)	0.0983	0.1630	0.0844	0.0466	0.0178	0.0011	0.0004
TOZ (Noz matm-cm)							
(212.0)	0.0195	0.0055	0.0231	0.0113	0.0013	0.0000	0.0000
(255.0)	0.0235	0.0066	0.0277	0.0136	0.0016	0.0000	0.0000
(298.0)	0.0274	0.0077	0.0324	0.0159	0.0018	0.0000	0.0000
(337.0)	0.0310	0.0087	0.0367	0.0180	0.0021	0.0000	0.0000
TH2O (Water Vapor gm/cm2 km)							
(0.010)	0.0000	0.0000	0.0000	0.0000	0.0006	0.0016	0.0010
(0.100)	0.0000	0.0000	0.0000	0.0000	0.0057	0.0155	0.0101
(0.590)	0.0000	0.0000	0.0000	0.0000	0.0335	0.0915	0.0594
(1.000)	0.0000	0.0000	0.0000	0.0000	0.0568	0.1551	0.1007
(10.000)	0.0000	0.0000	0.0000	0.0000	0.5678	1.5508	1.0068
TCO2	0.0000	0.0000	0.0000	0.0000	0.0000	0.0094	0.0035

Aerosol Characteristics:

Radial Limits	Rmin=0.02 μm; Rmax=5.04 μm; ΔR=0.04 μm
Refractive Index	1.54-0.01i